Proc. Natl. Conf. Theor. Phys. **35** (2010), pp. 209-220

STUDY ON LATTICE AND ELECTRONIC STRUCTURES AT THE SURFACE OF $BATIO_3$ THIN FILMS BY DFT METHOD

NGUYEN THUY TRANG, NGUYEN VAN CHINH,
BACH THANH CONG, NGUYEN HOANG LINH
Computational Materials Science Laboratory, Faculty of Physics,
Hanoi University of Science, Vietnam

Abstract. *In this paper, the density functional theory (DFT) study on nano-thin films of the most typical ferroelectric compound $BaTiO_3$ was presented. The results showed that the convergence of the film model using for DFT calculation were obtained for the thickness of the vacuum slabs as large as ten times of the $BaTiO_3$ slabs within the total energy error $\backsim$ 0.01 eV. The lattice contraction was observed in the surface region of the material. The difference in atomic layer termination, between BaO terminated and TiO_2 terminated films, gives rise to the difference in lattice reconstruction at the surface region which, in turn, leads to the difference in surface electric dipoles. The surface effect acts on the electronic structure of thin films in the manner of the asymmetry of atomic sites and the structural reconstruction due to the surface relaxation. Our results indicated that the termination also decides how and how much these two manners take effects on the electronic structure of the material.*

I. INTRODUCTION

Since the discovery of ferroelectric ceramics, chemically stable and relatively inert ferroelectric crystals have been widely recognized to be excellent candidates for electrically switchable, two-state devices... However, high switching voltages of several kV make thick crystal plates not favorable for commercial devices [1]. Then, the low-switching-voltage (only a few V) constructions like low-dimensional ferroelectric materials (for example: thin film of 100 $\div$ 800 nm in thickness [2], nanowire of several-tens nanometers in diameter [3]) are more suitable for practical electronic devices. In the trend of miniature high-density memory devices, the lower dimensions of material are, the more technologically meaningful the material becomes. Hence, the development of practical ferroelectric devices is in close connection with physics of low-dimension ferroelectric materials, of which, the most important problems are size and surface effects.

$BaTiO_3$ is a typical ferroelectric ceramic whose low-dimension effects on nanoparticles were first investigated by M. Anliker et al in 1954 [4]. A ferroelectric surface layer of about 20 nm was observed to remain ferroelectric far above the Curie temperature TC for $BaTiO_3$ single crystals of the size ranging from 30 to 2300 nm. This result was in contrast with later experiments, which have indicated the disappearance of tetragonal ferroelectric structure below a critical size varying from 5 to 120 nm [5, 6, 7, 8, 9, 10, 11]. The low-dimension effects occurring in nanowires of $BaTiO_3$ result in the reducing of ferroelectric-paraelectric phase transition temperature T_c with respect to the reducing of the wire cross section [12]. Z. Wang et al proposed a core shell model to explain the

preferred polarization orientation in $BaTiO_3$ nanowires [13]. They estimated the shell thickness of a nanowire with diameter of 120 nm to be $\backsim$ 10 nm. In this paper, we introduce our ab initio investigation on $BaTiO_3$ thin films to study the influence of the surface effect on the lattice and electronic structure of the material.

II. MODELLING

Among ab initio methods, Hartree-Fock method can be applied successfully for many systems. However, it also produces significant errors for wide range of other systems as it does not fully involve the correlation effect. Various methods have been developed to correct these errors basing on Hartree-Fock method (so-called Post-SCF methods) such as Moller-Plesset perturbation methods (MPn), quadratic configuration interaction methods (QCI), coupled cluster methods (CC), Brueckner doubles methods (BD) These methods make some improvements in calculation but they consume a lot of computational cost. Hence, methods based on Density Functional Theory (DFT) have been developed and popularized quickly. The best DFT methods achieve significantly greater accuracy with much less computational cost than the Post-SCF ones. DFT methods include full correlation effect in terms of exchange-correlation functionals. Many exchange-correlation functionals have been formulated in various forms which can be classified into three types: local approximation density (LDA) functional, generalized gradient approximation (GGA) functional and hybrid functional. In our calculation, we used a widely-used LDA func-

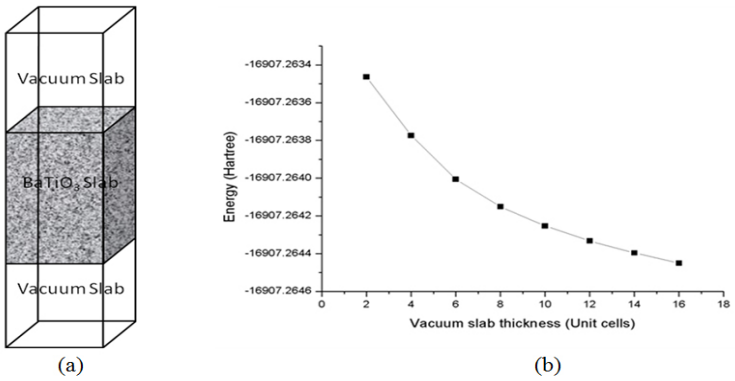

Fig. 1. (a) Supercell with $BaTiO_3$ and vacuum slab as a Q2D model; (b) The total energy dependence on VS thickness.

tional, PWC, which is proposed by Perdew et al [14]. The exchange-correlation functionals and local basis set were provided by the library of the quantum computing code $Dmol^3$, in which, all the atomic wave functions were given numerically in terms of atomic-centered spherical-polar meshes rather than analytic functions as Gaussian orbitals [15]. A full-electron potential was formulated from the all-electron wave function which includes all occupied atomic orbitals plus a second set of valence atomic orbitals and a polarization d-function on each atom by using DND basis set in $Dmol^3$'s library. A noticeable point is that almost of quantum computing codes, including $Dmol^3$, cannot treat two dimension (2D) structures. Then, a quasi-2D (Q2D) model is required to simulate $BaTiO_3$ thin

films. A supercell containing a vacuum slab (VS) and a $BaTiO_3$ slab (BS) (Fig. 1a) was built. This model preserves the periodicity in the slab plane (Oxy plane). However, the VSs prevent the wave functions of different BSs from overlapping and electrostatically interacting. By this way, the periodicity in the third dimension (Oz direction) is broken. Such Q2D model becomes ideal 2D model when the vacuum slab extends infinitely. In this work, we first examined the convergence of the one BS unitcell model ($\backsim 4\mathring{A}$) with respect to VS thickness in terms of total energy accuracy. Fig. 1b demonstrates the VS thickness-dependence of the total energy. The curve was fitted with an exponential decay function:

$$y = y_0 + A_1 e^{-(x-x_0)/t_1} + A_2 e^{-(x-x_0)/t_2}$$

Here, $y_0 = -16907.26476$ Ha, $x_0 = 2$ unit cells length, $A_1 = 6.1706 \times 10^{-4}$ Ha, $A_2 = 6.77321 \times 10^{-4}$ Ha, $t_1 = 3.980678$, $t_2 = 16.57242$, y is the total energy and x is the VS thickness. According to the function, when the VS thickness tends to infinitive, the total energy reduces exponentially to $y_0 = -16907.26476$ Hartrees. Then, within the error of $\backsim 0.0005$ Ha $\backsim 0.01$ eV, the VS thickness was fixed as much as ten times of BS thickness. We took optimizing calculation for bulk and film models. The non-optimized (optimized) film models are called unreconstructed (reconstructed) films.

III. RESULTS AND DISCUSSION

III.1. Lattice reconstruction and electric dipole moments

In this work, we aimed at $BaTiO_3$ thin films with crystallographic plane of (100) which are constituted of BaO and TiO_2 layers alternately. The model used for calculation has the BS thickness of 3 unit cells (7 oxide layers) $\backsim 12$ $\mathring{A}$ and the VS thickness of 30 unit cells $\backsim 12$ nm. Because the BS can be terminated with BaO or TiO_2 layers there are two film types: BaO-terminated (film A) and TiO_2-terminated (film B) (see Fig. 2). In each film, we have surface unit cell and centre unit cell which are denoted by s and c indexes, respectively. The oxide layers of the films are also numbered in Fig. 2. The center layer which is TiO_2 one for film A and BaO for film B is numbered 0. The odd numbers are BaO layers for film A, TiO_2 layers for film B and vice versa for even numbers.

The table 1 displays the lattice reconstruction parameters of $BaTiO_3$ films. The surface and centre unit cell volumes of the films are V_s and V_c, respectively. These values were compared with the bulk value V_{bulk} through the parameters: $V_s/V_{bulk} = (V_{bulk} - V_s)/V_{bulk}$ and $V_c/V_{bulk} = (V_{bulk} - V_c)/V_{bulk}$. Similarly for the TiO_6 octahedron volumes we have following quantities: ν_s, ν_c and $\Delta\nu_s/\Delta\nu_{bulk} = (\nu_{bulk} - \nu_s)/\Delta\nu_{bulk}, \Delta\nu_c/\Delta\nu_{bulk} = (\nu_{bulk} - \nu_c)/\Delta\nu_{bulk}$. In order to characterize the structural reconstruction of each oxide layer, we introduced a bumpiness quantity which is the difference between z coordinate of metal and oxygen atoms in each layer, i. e. the bumpiness of BaO layer is $\lambda_{BaO} = z_{Ba} - z_O$ and of TiO_2 layer is $\lambda_{TiO_2} = z_{Ti} - z_O$. It should be noted that we assumed the positive direction points to outward of the films. Then, some features of the lattice reconstruction and ionic electric dipole can be deduced from these parameters as following:

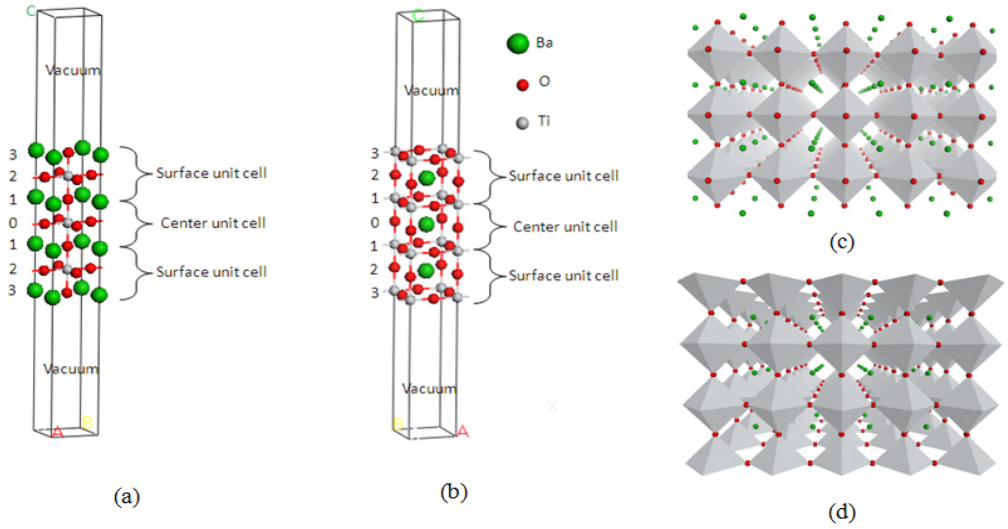

Fig. 2. The two BSs used for investigation: (a) BaO-terminated slab and (b) TiO_2-terminated slab; (c) and (d) are perspective views at 30^o along x direction of BaO-terminated and TiO2-terminated films in polyhedral form, respectively.

i. The lattice unit cell and TiO_6 octahedron trend to contract from the center to the surface. This contraction is in agreement with the bond-order-length-strength correlation proposed by C. Q. Sun et al [16] which has been evidenced by various experimental measurements [17, 18, 19]. Due to break of the periodicity in the direction perpendicular to the film surface, the atom system tends to reconstruct along this direction. During this process, the relative displacements of ions with different charges are different depending on their electronic structure and the surrounding opposite charged ions distribution.
ii. For the BaO-terminated film, the octahedron contracts less than the lattice unit cell while both lattice unit cell and octahedron of the TiO_2-terminated film contract the same. Moreover, the lattice contraction and reconstruction energy of the TiO_2-terminated film are much more than the BaO-terminated film.

iii. The contraction of both center and surface unit cells of studied films seems to in contrary with the experimental observation on the anomalous lattice expansion of nanocrystalline $BaTiO_3$ particles of S. Tsunekawa et al [11]. However, it should be noted that their experimental lattice parameters were averaged overall particles with smallest size of 20 nm which are much larger than the thickness of our model (3 unit cells $\backsim$12 nm). Then it is suggested that the BS of our model is not thick enough to get the best representation for the bulk-like properties.

iv. In both cases, the bumpiness of BaO layers is always negative, i.e. oxygen negative ions trend to emerge from the barium positive ion plane. The negative bumpiness gives rise to the negative values of electric dipole moment of BaO layers (table 2). Thus, the electric dipole moment vectors of BaO layers always point inwards.

v. Unlike BaO layers, TiO_2 layers have opposite bumpiness, and hence opposite electric dipole moment vectors in the two cases (table 2). While the titanium positive ions

Table 1. Lattice reconstruction parameters of BaTiO3 films due to the surface relaxation.

	Film A	Film B	Bulk
Lattice unit cell			
$V_s(\mathring{A}^3)$	61,2656	59,9600	
$V_c(\mathring{A}^3)$	61,2656	59,9600	62,4763
$\Delta V_s/V_{bulk}$	1,94%	4,03%	-
$\Delta V_c/V_{bulk}$	1,01%	2,53%	-
TiO_6 coordination			
$\nu_s(\mathring{A}^3)$	10,3574	9,9952	
$\nu_c(\mathring{A}^3)$	10,3994	10,1538	10,4142
$\Delta\nu_s/\nu_{bulk}$	0,55%	4,02%	-
$\Delta\nu_c\nu_{bulk}$	0,14%	2,50%	-
Reconstruction energy			
ΔE (meV)	111	355	-
Bumpiness of each oxide layer $(\mathring{A})$			
λ_3	-0,0713	-0,1012	
λ_2	0,0189	-0,0482	-
λ_1	-0,0172	-0,0115	
λ_0	0	0	

are convex outwards in the case of of BaO-terminated, they are concave inwards in the case of TiO_2-terminated. Thus, the electric dipole moment vectors of TiO_2 layers point outwards in the first case but inwards in the second. vi. According to (iv) and (v),

Table 2. The electric dipole moment per unit cell of each oxide layer (P_i, i = 0, 1, 2, 3) and the total surface electric dipole moment per unit cell of reconstructed films in e.$\mathring{A}$.

	Film A	Film B
P_3	-0,1717	-0,2829
P_2	0,0468	-0,1244
P_1	-0,0445	-0,0296
P_0	0	0
P_{total}	-0.1694	-0.4369

the dipole moments of TiO_2 layers and BaO layers are anti-parallel in the case of BaO termination and parallel in the remaining case. As a result, the total surface dipole of the BaO terminated film is smaller than the TiO_2 one.

vii. From the surfaces to centre, the bumpiness and dipole moment magnitude reduce quickly but remain non-zero value for all oxide layers except for central layer (no.0). The dipole moment value reduces about 73% from surface layer (no.3) to layer no.2 and 5% from layer no.2 to layer no.1 in the case of BaO terminated; 56% from surface layer to layer no.2 and 76% from layer no.2 to layer no.1 in the case of TiO_2 terminated.

III.2. Electronic structure

Fig. 3 represents the calculated density of states (DOS) of bulk and thin films. For all three investigated cases, four energy bands were obtained and numbered from 1

to 4. Table 3 shows in detail the location and peaks structure of these bands. It should be noted that the negative-energy bands no.1 and no.2 (the red dash line in the DOS) below Fermi level, which was normalized to 0 eV, are occupied and the positive-energy bands no.3 and no.4 are un-occupied. The difference between the DOS of bulk (Fig. 3b), unreconstructed (dot lines in Fig. 3c, d) and reconstructed films (solid lines in Fig. 3c, d) electronic structures suggests that the surface occurrence takes effect on the lattice and electronic structure of $BaTiO_3$ in two manners. One is that the surface occurrence breaks the periodic symmetry of the infinite crystal in the direction z perpendicular to the surface plane (Oxy), giving rise to the classification of atomic site into surface and subsurface sites along this direction which are so-call asymmetry sites. The other is that the crystal reconstruction due to the coordination number imperfection of surface atoms (the surface relaxation) leads to the re-contribution of the electronic structure.

The core band no.1 is mainly composed of Ba 4p states (the contributions of O and Ti are insignificant). For bulk material, it ranges from -11 to -9 eV with only one narrow, sharp peak at -9.9 eV (Fig. 3b). Due to the break of periodicity, the barium sites can be divided into surface (Ba^3) and subsurface (Ba^1) sites in the case of BaO-terminated film (film A) and Ba^2 and Ba^0 sites in the case of TiO_2-terminated film (film B) (Fig. 2). This asymmetry classification, in turn, splits the Ba 5p peak ion two peaks, i. e. the Ba^1 4p at -9.9 eV and the Ba^3 4p at -11.6 eV peak in the film A DOS (Fig. 3c). However, the splitting is unobvious in the case of film B with both Ba^2 and Ba^0 peaks locating around -10.7 eV (Fig. 3d). The surface structural reconstruction causes an insignificant change on the Ba core band of film A: no shift of peak 1b and only a small positive shift of peak 1a (0.1 eV). The shift of corresponding peaks of film B due to the structural reconstruction is $\backsim$0.3 eV down. Thus the surface takes effect on the electronic core band primarily in the manner of the asymmetry of atomic sites. The surface- and size- core-band splitting and shift have been observed experimentally in various compounds. Their proposed mechanisms were unclear and diverse. For example, the positive shifts of the core-electron binding energy level (corresponding with the negative shift of the DOS core band) of Nb 3d and T 4f were assigned to the enhancement of the resonance diffraction of the light due to the surface bond contraction [20, 21, 22]. The Cu 2p core-level shift of CuO nanosolid was explained as the size-enhanced ionicity of copper and oxygen [23]. C. Q. Sun et al have developed a bond order-length-strength correlation mechanism and unified the effects of surface relaxation and nanosolid formation on the core-level binding-energy shift into the atomic-coordination number imperfection [16, 24]. According to this, there are two highly favored mechanisms, i.e. the specification of the capping and surface layers in nanosolid which is in accordance with the positive shift of core levels and the surface relaxation [24]. Our calculation is in agreement with their conclusion that the asymmetry of barium sites or the specification of the capping and surface layers gives rise to the negative shift of the DOS core band of Ba 4p which is corresponding with the positive shift of the core-level binding-energy (the positive shift of the DOS core band is corresponding with the negative shift of the core-level binding-energy). Besides, according to our calculation, the termination layer is the important factor to decide how much the asymmetry splitting shifts the core level up and how the surface relaxation should shifts the core level. In the BaO termination case of $BaTiO_3$ films, the asymmetry of barium sites plays the prime role

Table 3. The location and DOS peak structure of energy bands of bulk material and under-investigation films in eV.

		Film A		Film B	
	Bulk	Unreconst.	Reconst.	Unreconst.	Reconst.
Band no.1	-11.0 ÷ -8.0	-12.3 ÷ -9.0	-12.3 ÷ -9.0	-12.0 ÷ -10.0	-12.3 ÷ -10.3
Peak 1a	-9.9	-11.6	-11.5	-10.7	-11.0
1b		-9.9	-9.9	-10.7	-11.0
Band no.2	-5.0 ÷ 0.0	-5.0 ÷ 0.0	-5.0 ÷ 0.0	-6.0 ÷ 0.0	-6.0 ÷ 0.0
Peak 2a	-4.1	-4.0	-4.2	-5.5	-5.5
2b	-3.6	-3.1	-3.4	-4.3	-4.6
2c	-2.5	-2.5	-2.5	-3.5	-3.9
2d	-	-	-	-2.7	-2.7
2e	-0.8	-0.6	-0.8	-1.6	-1.7
2f	-	-	-	-0.4	-0.6
Band no.3	1.8 (band gap value) ÷ 7.0	1.8 (band gap value) ÷ 8.0	1.8 (band gap value) ÷ 8.0	1.5 (band gap value) ÷ 6.5	1.2 (band gap value) ÷ 6.5
Peak 3a	2.0	2.4	2.4	1.5	1.3
3b	2.7	3.1	3.1	2.0	1.7
3c	3.7	3.7	3.7	2.7	2.6
3c'	-	-	-	-	3.2
3d	4.8	5.1	5.1	3.9	4.0
3e	-	5.5	5.5	4.9	4.8
3f	6.0	6.1	6.1	5.5	5.3
3g	6.8	6.9	6.9	6.2	6.0
3h	-	7.7	7.8		
Band no.3	≥7.0	≥8.0		≥6.5	

in the negative shift of the DOS Ba 4p band. The surface relaxation part is only significant but still smaller than the asymmetry part in the case of TiO_2 terminated $BaTiO_3$ films. Moreover, the surface relaxation tends to shift the DOS core-band slightly up in the case of BaO termination and down in the case of TiO_2 termination.

The high-energy un-occupied band no.4 which locates above 7 eV in the bulk DOS, 8 eV in the film A DOS and 6 eV in the film B DOS is mainly contributed by Ba valence states (5p and 6s) with only a small part from un-occupied O 2p and Ti 3d states (Fig. 3b, c, d).

The nearly non-overlap with Ti and O bands of the barium bands suggests that the bonding between barium atoms and the remaining part of lattice (TiO_6 octahedral network) is strongly ionic. This is also obvious in the calculated electron population which is shown in terms of (001) and (110) slices (Fig. 4). According to this, Ba atoms nearly do not share electron cloud with TiO_6 network. Mulliken's electron population analysis [25] produces the nearly ideal ionic charge values for barium ions (see table 4). It should be noted that if these bonds were ideally ionic the barium ionic charge would be $+2|e|$

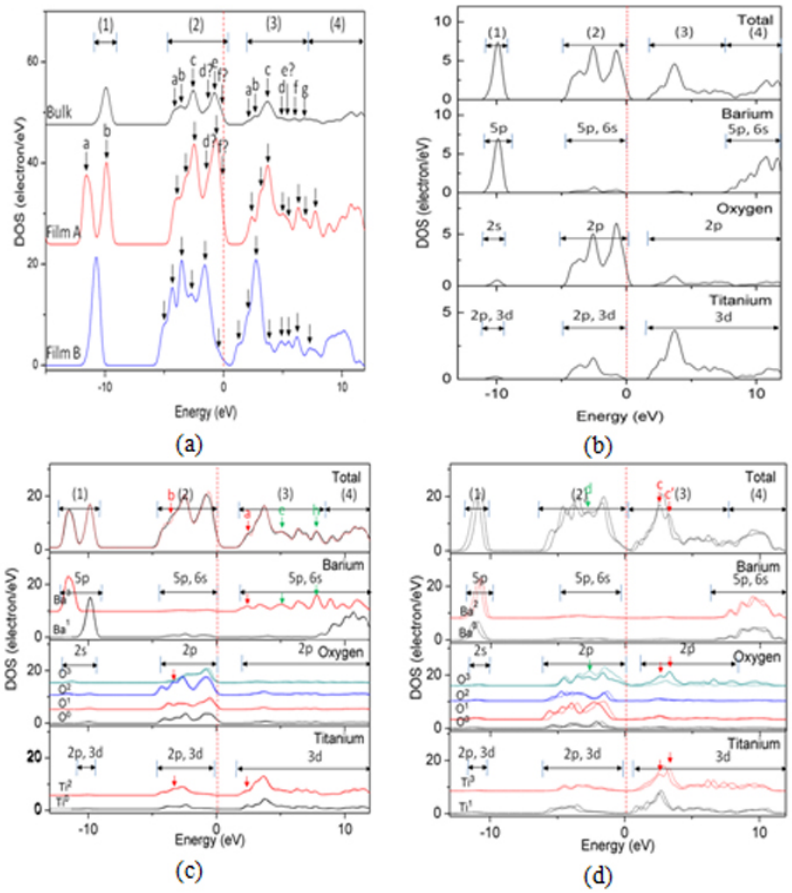

Fig. 3. (a) The DOS of $BaTiO_3$ calculated for 3D periodic model as bulk material (the top curve), non-optimized Q2D periodic models as unreconstructed thin films A and B (the mid and bottom curves respectively). The red dash line denotes Fermi level which was normalized to 0 eV. Below Fermi level bands no.1 and no.2 are occupied. Above Fermi level bands no.3 and no.4 are unoccupied. Bands no.2 and no.3 are the highest occupied and lowest unoccupied bands which are well-known as valence and conductive bands respectively. (b), (c), (d) The partial DOS curves for bulk material and reconstructed (solid lines) and unreconstructed (dot lines) films A, B respectively.

and $[TiO_3]$ ionic charge would be -2$|e|$. In the film A DOS, however, a noticeable Ba part ($\backsim$ 19%)appears in the lower-energy un-occupied band no.3 (conductive band) which is primarily constituted of Ti 3d and O 2p states (Fig. 3c).

This contribution originates from the surface site (Ba^3) due to the significantly overlap of Ba^3 valence orbitals with octahedral valence orbitals. This overlap strongly reduces the electric charge of the surface barium ions (from $\backsim$ +1.7$|e|$ for bulk Ba to $\backsim$ +1.4$|e|$ for surface Ba, see table 4). The Ba ionic charge reduction also occurs from

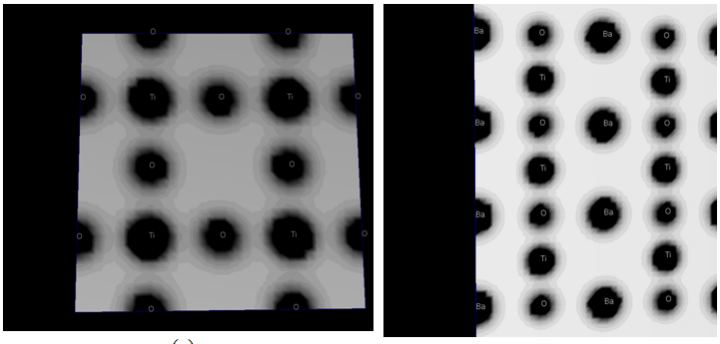

Fig. 4. Electron population in (001) and (110) slices ((a) and (b) respectively) of $BaTiO_3$ crystal lattice. The covalence nature of the bonds in TiO_6 octahedron was exposed by the fact that they share the valence electron clouds. The bonds between Ba atoms and TiO_6 network are primarily ionic.

Table 4. Atomic electric charge in |e|.

	Film A		Film B		
	Unreconstr.	Reconstr.	Unreconstr.	Reconstr.	Bulk
Ba^0	-		+1.830	+1.842	
Ba^1	+1.764	+1.736	-		+1.663
Ba^2	-		+1.728	+1.730	(charge)
Ba^3	+1.423	+1.456	-		
Ti^0	+0.863	+0.842	-		
Ti^1	-		+0.835	+0.901	+0.848
Ti^2	+1.728	+1.730	-		(charge)
Ti^3	-		+1.165	+1.095	
O^0	-0.843	-0.845	-0.841	-0.845	
O^1	-0.848	-0.845	-0.841	-0.837	-0.837
O^2	-0.853	-0.861	-0.836	-0.851	(charge)
O^3	-0.978	-0.952	-0.853	-0.850	

the center site to surface site but more slightly. The reducing of ionic charge of barium indicates the change of the bonding nature from ionic to valence. Thence, there occurs the change in nature of the Ba-[TiO_6] bonding from ionic to valence in the surface region of the material and the phenomenon is the most obvious in the case of BaO termination where the outmost layer contains Ba ions. The ionic-valence transformation of the surface Ba-[TiO_6] bonding has been also experimentally observed by means of XPS spectroscopy on nanocrytalline $BaTiO_3$ particles [11]. The calculation in [11] did not clarify whether the origin of the bonding nature modification is the asymmetry splitting of barium site or the surface relaxation. The insignificant effect on the barium ionic charge in our results suggests that this modification directly originates from the asymmetry of barium sites rather than the surface relaxation.

Valence and conductive bands are composed of hybrid states between O 2p and Ti 3d orbitals. So TiO_6 octahedral coordination is the most important to the electronic structure

of the material. The valence band no.2 is constituted similarly for bulk and films with a large O 2p part (∽76%), a smaller Ti part (∽17%) and an insignificant part (∽7%) of Ba 6s, 5p orbitals. In contrary with the valence band, conductive band has a large part of titanium 3d orbitals (82% for bulk and film B, 65% for film A). The remaining part comes from O 2p orbitals in the case of bulk and film B. For film A in particular (as has been discussed above), the remaining part has 46% O 2p character and 54% Ba 5p, 6s character which comes from the surface site (Fig. 3c). However, the bonds in TiO_6 octahedral network of all three cases are essentially valence. The valence nature is corresponding to the small electric charge values of titanium and oxygen (table 4) and obviously displayed in Fig. 4. According to this, the TiO_6 octahedral network exhibits itself as positive charged core parts of titanium and oxygen atoms sharing a valence electron cloud. In this network, the charge transfer has been both experimentally and computationally evidenced to occur between different TiO_6 octahedral clusters rather than atom by atom [26, 27, 28]. Then, the break of the TiO_6 octahedral coordination at the surface should lead to a larger structural reconstruction in the case of TiO_6 terminated film than the BaO one as shown above. Due to the conservation of TiO_6 octahedral coordination at the surface of film A, the asymmetry of Ti and O sites only lead to some small change of the O 2p - Ti 3d hybrid bands without the shift of the highest peaks no.2c and 3c.The slight shift and enhancement are observed on some weaker peaks. The most visible shift (about 0.4 eV - table 3) and enhancement occurs for 2b and 3a peaks which are contributed by TiO_2 layers no.2 and surface barium states respectively (denoted by red arrows in Fig. 3c). Besides the additional peaks no.3e at 5.5 eV and 3h at 7.7 eV originate from the surface barium atoms (green arrows in Fig. 3c).

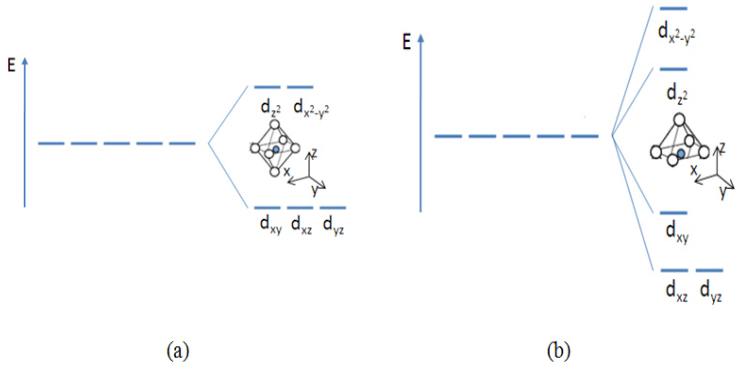

Fig. 5. The splitting of 5 d orbitals in the crystal fields of octahedron (a) and pyramid (b).

The scene is not the same for the film B because the crystal field splitting is much different between octahedral and pyramidal coordinations as seen in Fig. 5. Of course, the case should be much more complicated in $BaTiO_3$ crystalline films where other splitting processes may also occur such as bonding-antibonding splitting, asymmetry splitting The result is the band gap reducing, the downward broadening of both valence and conducting bands and two additional peaks at -2.7 and -0.4 eV (no.2d and 2f) which have the origin of

the asymmetry of the pyramidal-bottom oxygen O^3 (green arrows in Fig.3d). The surface relaxation gives rise to a small change in the TiO_6 bands of film A with an insignificant band gap change and small peak shifts but a quite obvious change in those ones of film B with a reduced band gap and some additional peaks. The contraction of the TiO_6 octahedron increase the overlap of Ti 3d and O 2p orbitals which enlarges the bonding-antibonding splitting of the hybridized orbitals. Then the 0.55% contraction of the surface TiO_6 octahedron is corresponding to the slightly-negative shift ($\backsim$0.3 eV) of valence band peaks and the non-shift of conductive band peaks in the case of film A. In the film B case, the larger contraction ($\backsim$ 4.02%) together with the break of TiO_6 octahedral coordination into TiO_5 pyramidal coordination not only enlarges the bonding-antibonding gap but also enhances the crystal splitting. Then in addition to the peak shifts (almost is negative), we observed a new satellite of the highest peak of the conductive band no. 3c at 3.2 eV (no. 3c' which denoted by red arrow in Fig. 3d) which originates from the bottom of the TiO_5 pyramid (Ti^3 and O^3).

IV. CONCLUSION

We have investigated the surface effect of $BaTiO_3$ using Q2D model. Our results are qualitatively in agreement with some experimental observation and bond order-length-strength correlation model by C. Q. Sun et al [16]. According to this, the surface effect act on the electronic structure of the material in two manners. Firstly, the surface occurrence leads to the asymmetry of the atomic sites along the direction perpendicular to the film plane. This asymmetry is respondsible for the splitting and negative shift of DOS core band and plays the main role in the slight change of bonding nature in the surface region of $BaTiO_3$. The other manner is the structural reconstruction due to the surface relaxation which enhances the bonding-antibonding and crystal field splitting of TiO_6 orbitals. The comparison between the TiO_2 terminated and BaO terminated films suggests that the termination is the key factor to define how and how much the two manners take effect on the lattice and electronic structures of thin films. It is well evidenced that due to the break of the TiO_6 octahedral coordination into TiO_5 pyramidal one at the surface the lattice and the electronic structures of TiO_2 terminated films were modified much more than the BaO terminated ones. Moreover, the termination is also the importance factor to predict the surface electric polarization properties of $BaTiO_3$: the surface polarization of TiO_2 terminated films is larger than the BaO ones.

ACKNOWLEDGEMENT

We would like to thank the project No. QGTD09-05 for financial support.

REFERENCES

[1] G. A. Samara, *Phys. Rev.* **151** (1996) 378.
[2] H. F. Kay, J. W. Dunn, *Philos. Mag.* **7** (1962) 2027.
[3] S. G. Jayama, K. Navaneethakrishnan, *J. App. Phys.* **89** (2001) 6198.
[4] M. Anliker, H. R. Brugger, W. Kaenzig, *Helv. Phys. Acta* **27** (1954) 99.
[5] R. Bachmann, K. Baerrer, *Solid state Comm.* **68(9)** (1988) 865.
[6] K. Uchino, E. Sadanaga, T. Oonish, T. Morohashi, H. Yamamoto, *Ceram. Transaction* **8** (1990) 107.

[7] T. Yamamoto, K. Urabe, H. Banno, *Japanese Journal of Applied Physics* **32** (1993) 4272.
[8] M. H. Frey, D. A. Payne, *Appl. Phys. Lett.* **63(20)** (1993) 2753.
[9] K. Saegusa, E. R. Wendell, H. K. Bowen, *J. Am. Ceram. Soc.* **76(6)** (1993) 1505.
[10] S. Schalag, H. F. Eicke, *Solid state Comm.* **91(11)** (1994) 883.
[11] S. Tsunekawa, S. Ito, T. Mori, K. Ishikawa, Z. Q. Li, Y. Kawazoe, *Physical Review B* **62(5)** (2000) 3065.
[12] J. E. Spanier, A. M. Kolpak, J. J. Urban, I. Grinberg, L. Ouyang, W. S. Yun, A. M. Rappe, H. Park, *Nanoletters* **6(4)** (2006) 735-739.
[13] Z. Wang, J. Hu, M. F. Yu, *Nanotechnology* **18** (2007) 235203.
[14] J. P. Perdew, Y. Wang, *Phys. Rev. B* **45** (1992) 13244.
[15] B. Delley, *J. Chem. Phys.* **92** (1990) 508.
[16] C. Q. Sun, B. K. Tay, X. T. Zeng, S. Li, T. P. Chen, J. Zhou, H. L.Bai, E. Y. Jiang, *J. Phys.: Condens. Matter* **14** (2002) 7781.
[17] C. Q. Sun, *Surf. Rev. Lett.* **8** (2001) 367.
[18] Qian, W. Hubner, *Phys. Rev. B* **60** (1999) 16192.
[19] W. T. Geng, A. J. Freeman, R. Q. Wu, *Phys. Rev. B* **63** (2001) 064427.
[20] B. S. Fang, W. S. Lo, T. S. Chien, T. C. Leung, C. Y. Lue, C. T. Chan, K. M. Ho, *Phys. Rev. B* **50** (1994) 11093.
[21] T. Balasubramanian, J. N. Andersen, L. Wallden, *Phys. Rev. B* **64** (2001) 205420.
[22] R. A. Bartynski, D. Heskett, K. Garrison, G. Watson, D. M. Zehner, W. N. Mei, S. Y. Tong, X. Pan, *J. Vac. Sci. Technol. A* **7** (1989) 1931.
[23] K. Borgohain, J. B. Singh, M. V. R. Rao, T. Shripathi, S. Mahamuni, *Phys. Rev. B* **61** (2000) 11093.
[24] C. Q. Sun, *Phys. Rev B* **69** (2004) 045105.
[25] R. S. Mulliken, *J. Chem. Phys.* **23** (1955) 1833-1846.
[26] S. Lenjer, O. F. Schirmer, H. Hesse, Th. W. Kool, *Phys. Rev. B* **66** (2002) 165106.
[27] R. I. Eglitis, E. A. Kotomin, G. Borstel, *J. Phys. Condens. Matter* **14** (2002) 3735.
[28] H. Pinto, A. Stashans, *Phys. Rev. B* **65** (2002) 134304.

Received 28-09-2010.